

Zone-axis x-ray diffraction of single-crystal Fe_{1-x}O under pressure

Yang Ding,^{1,*} Haozhe Liu,¹ Maddury Somayazulu,¹ Yue Meng,¹ Jian Xu,¹ Charles T. Prewitt,²
Russell J. Hemley,¹ and Ho-kwang Mao¹

¹*Geophysical Laboratory, Carnegie Institution of Washington, 5251 Broad Branch Road, N.W., Washington, D.C. 20015, USA*

²*Department of Geosciences, University of Arizona, Tucson, Arizona 85721, USA*

(Received 25 March 2005; revised manuscript received 8 June 2005; published 10 November 2005)

Zone-axis synchrotron x-ray diffraction of single-crystal Fe_{1-x}O to 25 GPa is used to study the effect of pressure on the defect cluster superstructure and to obtain further details on the cubic-to-rhombohedral phase transition in this material. Fe_{1-x}O is found to exhibit a pressure-induced long-range order-disorder transition of defect clusters as the satellite reflections originating from an incommensurate defect superstructure disappear around 14.0 GPa. The wave vectors of the incommensurately modulated defect structure increase with pressure, while the intensity of incommensurate peaks decreases. In contrast to temperature-induced order-disorder transitions, the pressure-induced transition is not reversible. Additionally, twinning is unambiguously observed to accompany the transition from a cubic to a rhombohedral phase at 19.8 GPa.

DOI: [10.1103/PhysRevB.72.174109](https://doi.org/10.1103/PhysRevB.72.174109)

PACS number(s): 61.50.Ks, 62.50.+p, 64.70.Kb

I. INTRODUCTION

Fe_{1-x}O , (wüstite) is a nonstoichiometric iron oxide with a rocksalt (B1) type basis crystal structure that is incommensurately modulated with a long-range ordered defect structure.^{1,2} Fe_{1-x}O is of fundamental importance in condensed-matter physics, chemistry, and earth science.^{3,4} Two high-pressure phase transformations have been observed from previous powder diffraction studies. The first one is from the ambient pressure B1 phase to a rhombohedral phase near 15–18 GPa at room temperature,^{5–7} and the other one is from rhombohedral to a B8 (or anti-B8) phase around 74 GPa at 900 K.⁸ At ambient pressure, the observation of the superstructure reflections incommensurate with the main reflections has been attributed to the ordering of defect clusters associated with octahedral cation vacancies and tetrahedral interstitial Fe^{3+} (Refs. 1 and 2). Although the exact defect structure is still a matter of much debate, there is substantial experimental and theoretical evidence that by edge or corner sharing a 4:1 cluster can form larger and more stable 6:2, 8:3, 13:4, 16:5, ... etc., defect clusters.⁹ It is common to observe that the defect clusters have an incommensurate spacing $\sim 2.6a_0$, where a_0 is the basic Fe_{1-x}O rocksalt lattice parameter.^{1,2} The existence of diffuse scattering besides the superstructure reflections suggests the modulated structure should be regarded as a paracrystal-like distribution of defects,² rather than a perfect periodic structure. However, the high-pressure study of the incommensurate defect superstructure is not yet available because it is not possible to obtain information on defect superstructure directly through

routine high-pressure powder diffraction techniques. In this paper, by applying the zone-axis single crystal diffraction method, we not only discovered a long-range order-disorder phase transition of defect clusters at around 14.0 GPa (from the pressure dependence of superstructure reflections and their disappearance at higher pressures), but also clarified the spatial symmetry changes in Fe_{1-x}O near 20 GPa associated with the transformation from the cubic to the rhombohedral phase.

II. ZONE-AXIS DIFFRACTION

Zone-axis diffraction of thin crystals is a powerful technique in transmission electron microscopy,¹⁰ but has seldom been applied with x rays^{11,12} because it can only be observed with thin crystals using short wavelength radiation. With the availability of high-energy x-ray synchrotron sources, there is the prospect of applying this technique in high-pressure diamond anvil cell experiments. Zone-axis diffraction provides rich spatial symmetry information that is lost in powder diffraction with only a single diffraction pattern. With the projection symmetries in the zone-axis diffraction patterns, certain ambiguities in high-pressure powder diffraction can be easily solved. More importantly, the zone-axis diffraction technique is especially suitable for studying single crystals at ultrahigh pressure because only very thin single crystals can survive at ultrahigh pressures.

Zone-axis diffraction patterns form when short wavelength radiation is parallel to the zone axis of a thin crystal, and it can be treated as transmission Laue diffraction. Under the single scattering approximation,¹⁰ the scattering intensity can be expressed as

$$I(K) \propto \left[(N_x N_y N_z V)^2 \frac{\sin^2(\pi N_a \vec{K} \cdot \vec{a})}{(\pi \vec{K} \cdot \vec{a})^2} \frac{\sin^2(\pi N_b \vec{K} \cdot \vec{b})}{(\pi \vec{K} \cdot \vec{b})^2} \frac{\sin^2(\pi N_c \vec{K} \cdot \vec{c})}{(\pi \vec{K} \cdot \vec{c})^2} \right] |F(\vec{K})|^2,$$

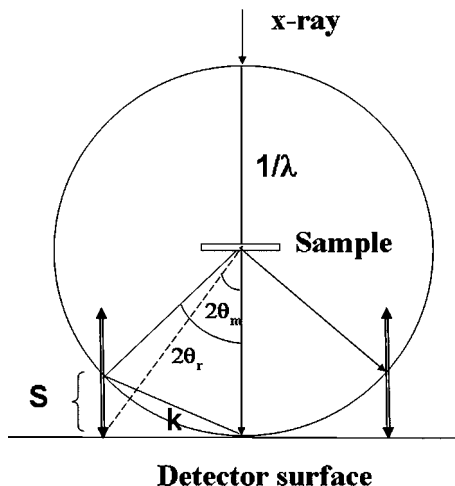


FIG. 1. The Ewald sphere construction for demonstration of zone-axis pattern formation. S : the excitation error, which is the length of the deviation of the measured Laue angle from the true Laue condition in reciprocal space (\AA^{-1}); k : scattering vector in \AA^{-1} ; $2\theta_m$: the measured Laue angle by FIT2D; $2\theta_r$: the true diffraction angle; λ : wavelength of the radiation.

where $F(K)$ is the structure factor of the crystal and the rest of the equation is the shape function of the crystal. N_x , N_y , and N_z are the numbers of cells along axes a , b , and c in real space, respectively, while K is a scattering vector in reciprocal space. One can estimate the thickness of the sample that would provide large enough excitation error for the observation of the diffraction pattern. The number of cells in the x and y directions is assumed to be much larger than that in the z direction, and can be approximately considered to be infinite for convenience of the estimation. It can be estimated that if the thickness of the Fe_{1-x}O sample is less than $20\ \mu\text{m}$ (about 5000 cells) along the z (x -ray beam) direction, then the length of diffraction rods of 220 with $0.4\ \text{\AA}$ wavelength synchrotron x -ray can be larger than the excitation error, i.e., the distance from the Laue diffraction to the flat surface of the detector, of $0.08\ \text{\AA}^{-1}$ (Ref. 13) and thus can intersect with the detector surface (Fig. 1). Therefore, some intensity of the 220 class diffraction can be recorded on a flat two-dimensional detector, even though the Laue condition is not exactly satisfied. The excitation errors, due to the deviation from Laue condition, can be corrected in d spacing measurement as

$$d_{\text{real}} = d_{\text{measured}} * \frac{1}{\cos \theta_{\text{measured}}}.$$

III. EXPERIMENTAL PROCEDURE

The Fe_{1-x}O sample was prepared by cold-pressing reagent-grade hematite (Fe_2O_3) into centimeter-sized pellets. The hematite pellets were held for ~ 24 h at $1200\ ^\circ\text{C}$ and 10 – 11 bar f_{O_2} in a CO/CO_2 gas-mixing furnace. The formation of magnetite during cooling was avoided by drop-

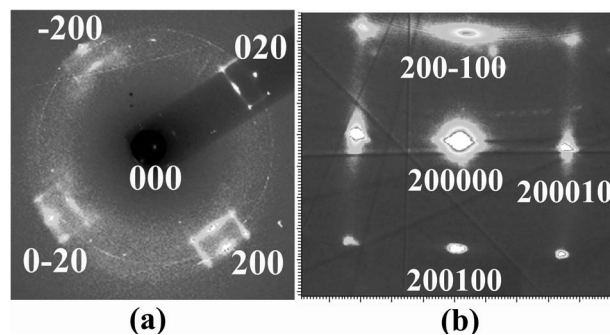


FIG. 2. (a) $\langle 100 \rangle$ The zone-axis pattern of Fe_{1-x}O with the main peaks indexed according to the $B1$ structure at ~ 1.0 GPa. The diffraction peaks around the class 200 peaks arise from an incommensurately-ordered defect structure (only four out of eight modulation reflections are visible). (b) Enlarged view of the incommensurate superstructure peaks (or modulation reflections) and diffuse scattering around the 200 000 peak at 1.6 GPa (all eight modulation reflections are visible). The indexing of the peaks is based on the notation of Yamamoto (Ref. 16).

quenching the sample into a separate container with the same gas mixture. The cell parameter of the Fe_{1-x}O was measured by conventional single crystal x -ray diffraction to be $a = 4.303(2)\ \text{\AA}$, corresponding to $\text{Fe}_{0.93}\text{O}$.¹⁴ High pressures were generated between two gem-quality single-crystal diamonds with $400\ \mu\text{m}$ culets in a symmetric diamond anvil cell. One single crystal of Fe_{1-x}O about $70 \times 35 \times 20\ \mu\text{m}^3$, cut along the $\{100\}$ plane, was placed into a $120\ \mu\text{m}$ hole that was drilled in a $45\text{-}\mu\text{m}$ -thick indentation of stainless steel gasket. One ruby chip ($\sim 20\ \mu\text{m}$ in diameter) was added as a pressure calibration standard, and a 4:1 methanol-ethanol mixture was used as the pressure medium. The diffraction experiments were performed at beamline 16-IDB, HPCAT (High Pressure Collaborative Access Team) of the APS (Advanced Photon Source), at Argonne National Laboratory. The monochromatic beam at $29.3\ \text{keV}$ was focused to about $20 \times 20\ \mu\text{m}^2$. The diamond anvil cell was mounted on a stage that could be rotated up to 10° around the vertical and horizontal axes for alignment purpose. Zone-axis diffraction patterns were taken along the $\langle 100 \rangle$ zone axis of cubic Fe_{1-x}O and recorded with a Mar345 image plate. Diffraction data were analyzed with the FIT2D program.¹⁵

IV. RESULTS

Zone-axis diffraction from a Fe_{1-x}O crystal in a diamond anvil cell revealed a diffraction image shown in Fig. 2(a). The strongest diffraction peaks show $4\ \text{mm}1_R$ symmetry, which is compatible with the projection symmetry of the cubic Fe_{1-x}O structure. Surrounding each fundamental peak of 200 family are superstructure peaks composed of a sharp diffraction peak and diffuse scattering along $\langle 100 \rangle$ directions, where only four out of eight superstructure peaks around each fundamental peak are visible in Fig. 2(a). Enlarged images of superstructure reflections obtained at 1.6 GPa are shown in Fig. 2(b), which was taken near the Bragg condi-

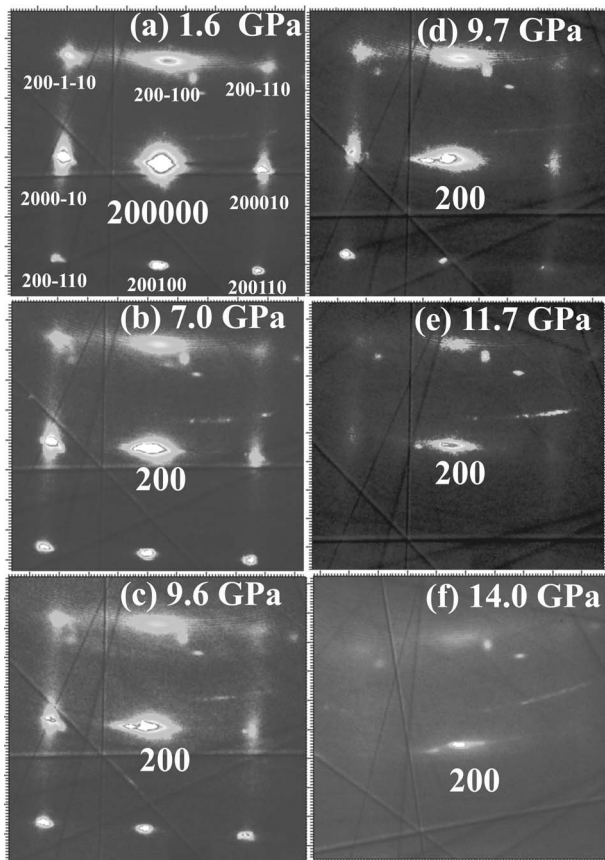


FIG. 3. The images of the main 200 reflection and the eight surrounding modulation reflections taken at pressures of (a) 1.6 GPa, (b) 7.0 GPa, (c) 9.6 GPa, (d) 9.7 GPa, (e) 11.7 GPa, and (f) 14.0 GPa. Indices based on the Yamamoto notation (Ref. 16) are shown in (a) for the main and modulation reflections.

tion of the 200 peak by tilting the crystal a few degrees away from the zone axis, so that all eight superstructure peaks around the fundamental 200 peak are visible. The structure of the incommensurate Fe_{1-x}O structure can be described by a six-dimensional space group $P_{Pm\bar{3}m}^{Fm\bar{3}m}$, (Ref. 16) and the incommensurately ordered defect structure can be mathematically described by a three-dimensional defect density modulation wave with incommensurate wave vectors $\mathbf{k}^1=0.377\mathbf{a}^*$,

$\mathbf{k}^2=0.377\mathbf{b}^*$, $\mathbf{k}^3=0.377\mathbf{c}^*$, where \mathbf{a}^* , \mathbf{b}^* , \mathbf{c}^* are the unit vectors in the reciprocal lattice of the basic structure. All diffraction reflections (including main and satellite reflections) are indexed using six integers h_1-h_6 according to $\mathbf{h}=h_1\mathbf{a}^*+h_2\mathbf{b}^*+h_3\mathbf{c}^*+h_4\mathbf{k}^1+h_5\mathbf{k}^2+h_6\mathbf{k}^3$ (Ref. 16). The h_1-h_6 indices for some of the modulation reflections and the main reflection are shown in Fig. 2(b).

The zone-axis diffraction images of the main 200 000 peak and its surrounding modulation peaks taken between 1.6 GPa and 14.0 GPa are displayed in Fig. 3. The wave vector value n (equal to 0.377 at ambient pressure) can be determined as a function of pressure from measuring the position of the satellite reflection 200 100, 200 010, etc., and the position of the main reflection 200 000 at different pressures. The pressure dependence of the modulation vector value n is shown in Fig. 4(a). It is obtained from the averaging of the wave vector values obtained from different satellite reflections around the 200 000 reflection, and it exhibits a slight scattering of values in the range of ± 0.001 . Figure 4(a) shows that the value of the wave vector increases with pressure. At the same time, the intensity of satellite diffraction peaks and the diffuse scattering around them decrease gradually with pressure (Fig. 3). Above 14.0 GPa, the satellite peaks and the diffuse scattering disappear, which indicates that a long-range order-disorder transition occurs. Wave vector values ($n=k/a^*$) increasing with pressure suggests that the periodicity of the averaged defect cluster superstructure decreases faster than that of Fe-O basis structure, and meanwhile, the intensity decreasing indicates that the coherence of modulation waves decreases with compression.

Through the long-range order-disorder transition, the Fe_{1-x}O single-crystal remains in the B1 phase, which is observed to be stable up to 19.8 GPa, where a phase transformation to a rhombohedral structure is observed. Figure 5 shows two zone-axis diffraction patterns of Fe_{1-x}O taken at 18.9 GPa and 25.2 GPa, respectively. The pattern in Fig. 5(a) displays a 4 mm_R projection symmetry, which is the same as that of patterns at ambient condition and indicates a cubic phase with symmetry $Fm\bar{3}m$. The lattice parameter a is determined as 4.1551(4) Å at 18.9 GPa. The indexing and simulated pattern of the cubic phase along a $\langle 100 \rangle$ zone axis is also displayed in Figs. 5(a) and 5(c). After a phase transformation at around 19.8 GPa, the pattern [Fig. 5(b)] shows splitting of class 220 peaks, but no splitting of class 200

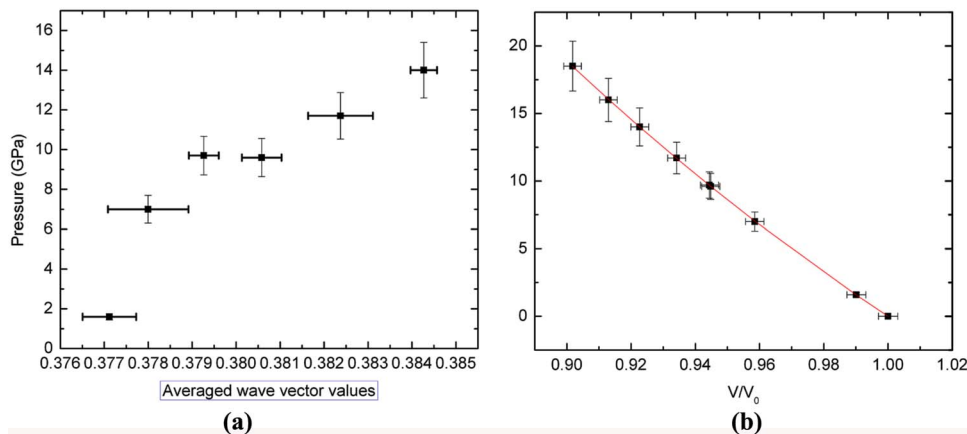


FIG. 4. (Color online) (a) The pressure dependence of the wave vector up to 14.0 GPa. (b) Fitting of pressure-volume data to the third order Birch-Murnaghan EOS; the resulting K_0 and K_0' are 156.7 (6.5) GPa and 2.6 (0.5), respectively. The atomic or cell volume at ambient condition is 79.673(9) Å³.

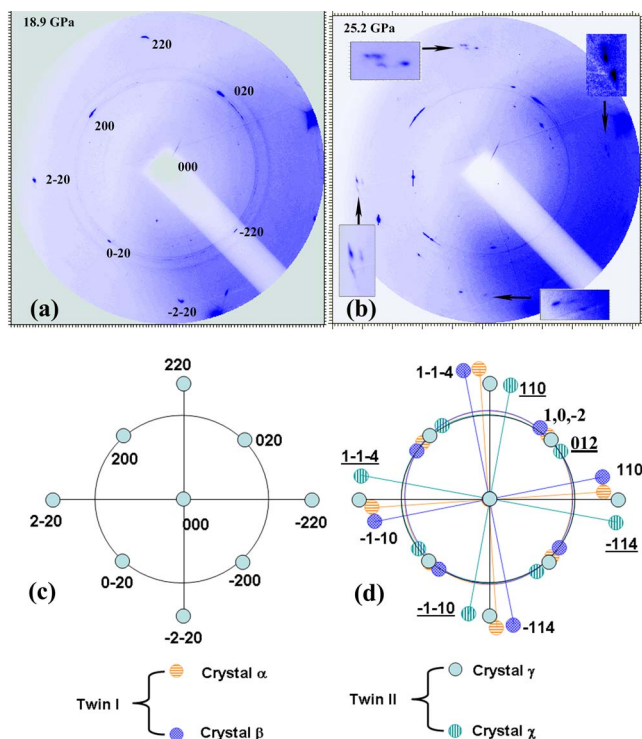


FIG. 5. (Color online) (a) Experimental diffraction pattern at 18.9 GPa, indexed based on cubic symmetry $Fm\bar{3}m$. (b) Experimental diffraction pattern at 25.2 GPa that shows the change of symmetry after the phase transformation occurring at about 19.8 GPa. (c) Simulation of a $\langle 100 \rangle$ zone-axis pattern of the cubic $Fe_{1-x}O$ phase. (d) Simulation of the experimental pattern of Fig. 5(b). The diffraction spots are indexed according to a $\langle 2, -2, 1 \rangle$ zone axis of rhombohedral symmetry. The underlined indices are from the other twin domain, and the α , β , γ , and χ crystals in twins I and II domains are used to simulate the mosaic spread. The powder diffraction rings in Figs. 5(a) and 5(b) are from the stainless steel gasket.

peaks. The splitting of class 220 peaks could be a result from a twinning of rhombohedral domains, which commonly occurs during structural phase transformation due to symmetry breaking. After $Fe_{1-x}O$ slightly deforms into rhombohedral symmetry ($R\bar{3}m$) by stretching along body diagonals, the $\langle 100 \rangle$ zone-axis pattern of cubic symmetry can be indexed as the $\langle 2, -2, 1 \rangle$ zone axis of rhombohedral symmetry, and diffraction class 200 and 220 of cubic symmetry can be indexed as class 012 and 110 (and -114) of rhombohedral symmetry, respectively. Since the c/a ratio of the rhombohedral phase is not equal to $\sqrt{6}$ (which corresponds to cubic symmetry), the d spacings of class 110 and class -114 are not equal. One can assume that the twinning of rhombohedral domains occurs in such a way [Fig. 5(d)] that the twin domains share the same zone axis $\langle 2, -2, 1 \rangle$ and have the same lattice parameters, but with nearly 90° difference in orientation along the zone axis. In this case, the diffraction 110 of one twin domain and diffraction -114 of the other twin domain are nearly parallel, but with different d spacings, which can result in splitting of class 220 after phase transformation. Since twin domains have same lattice parameters and cubic class

200 can only become class 012 of rhombohedral symmetry, there is no splitting of class 200 as observed in Fig. 5(b). In Fig. 5(d), two crystals with an offset of a few degrees in orientation along the zone axis are plotted in each twin domain to simulate the mosaic spreads as observed in Fig. 5(b). According to the above analysis and indexing, the lattice parameters of the twin domains of the rhombohedral structure are determined as $a=2.8529(3)$ Å and $c=7.4425(3)$ Å in an hexagonal setting (for rhombohedral setting, the lattice parameters are $a=2.1933$ Å and $\alpha=54.80^\circ$) at 25.2 GPa.

The transformation of $Fe_{1-x}O$ from the $B1$ to the rhombohedral structure is associated with softening of the elastic modulus C_{44} under pressure.^{1,17,18} The observation in this study has verified the previously proposed twinning in $Fe_{1-x}O$ at the phase transition.³ However, the assignment of four twin domains was uncertain due to the lack of spatial symmetry information in their experiments. For example, diffraction peaks from B and D domains³ had the same d spacing and the splitting could arise from the mosaic spread. In contrast, the mosaic spread and twin domains can be clearly discerned from zone-axis patterns in this study, and only two twin domains were observed.

The equation of state for the $Fe_{1-x}O$ cubic structure (determined from diffraction reflection 200) is shown in Fig. 4(b). No change in compression has been observed through the order-disorder phase transition at 14.0 GPa. The superstructure reflections have not reappeared on release of pressure, indicating that the transition is irreversible.

V. DISCUSSION

The discovery of the order-disorder defect-cluster transition indicates that the long-range ordered defect clusters either grow into larger long-range disordered clusters or dissolve to smaller long-range disordered clusters after transition pressure. According to lattice energy calculations, pressure can stabilize the defect clusters due to the defect cluster-cluster interactions,^{19,20} it is thus likely that the transition observed under high-pressure arises from defects growing into larger but less ordered clusters or eventually two-dimensional defects, such as stacking faults, after transition pressure.

This pressure-induced long-range order-disorder transition of defect clusters in $Fe_{1-x}O$ on compression (14.0 GPa) has not been reported before, though such a transition has been observed at ambient pressure at high temperature (at 650 K).²¹ The high-temperature-induced order-disorder transition is reversible on lowering temperature, but the pressure-induced one is not reversible on release of pressure. This suggests that these two transitions should result from different mechanisms. The temperature-induced transition could be a second-order displacive order-disorder transition and mainly driven by the gain of configurational entropy at increasing temperature. In contrast, the pressure-induced transition is possibly a first-order diffusional order-disorder transition and probably results from energy reduction associated with interactions between defects, such as octahedral Fe^{3+} , octahedral vacancies, and tetrahedral Fe^{2+} . Accordingly, defect clusters dissolve into smaller defects at elevated tem-

perature, whereas they grow into larger defects under compression. It is possible that there is a critical point existing in the range from 300 K/17.2 GPa to 650 K/1 bar.

No change of bulk modulus has been observed after the long-range order-disorder transition occurs [Fig. 4(b)], which is in contrast to the conjecture by Zhang²² but consistent with conclusions from Fei²³ and Haavik *et al.*²⁰ This observation can be considered as another evidence to indicate that the defect structure or nonstoichiometry has negligible (or minor) effects on the compressibility of Fe_{1-x}O.

The discovery of the pressure-induced defect order-disorder transition in Fe_{1-x}O may provide clues to the long-standing fundamental problems of its magnetic and structural phase transitions mechanism under high pressure. It is known that the transformation of Fe_{1-x}O from the *B1* to the rhombohedral structure is associated with softening of the elastic modulus C_{44} under pressure, but the driving force for the softening, which is considered to be magneto elastic coupling, is still under debate.²⁴⁻²⁶ High-pressure Mössbauer-Raman experiments indeed observed that magnetic transition accompanied the structural phase transition of Fe_{1-x}O above 14 GPa, but the high-pressure neutron diffraction did not detect any magnetic peak up to 20 GPa. The contradictory results between spectroscopy and diffraction methods indicate that the magnetic ordering transition occurs in short-range local structures but not in long-range order in Fe_{1-x}O. If one considers the fact that defect clusters in Fe_{1-x}O could have a magnetic structure,²⁷ it is natural to relate the magnetic transition observed by Mössbauer-Raman above 14 GPa with the defect cluster order-disorder transition that is found in the present work to occur around the same pressure. Thus, it is possible that above the pressure of the order-disorder transition, the larger but less ordered clusters form certain magnetic structures that can be detected by Mössbauer-Raman spectroscopy (for short-range magnetic ordering) but not neutron diffraction (for long-range magnetic ordering).

Meanwhile, most powder diffraction experiments of Fe_{1-x}O have found that the peak 111 starts to broaden around 14 GPa (under nearly hydrostatic conditions) before the

cubic-to-rhombohedral phase transition is completed. The peak broadening is usually considered to be a sign for the distortion of cubic to rhombohedral symmetry, also nearly occurring at the same time with the defect cluster order-disorder transition which is known to occur at an almost the same pressure as the defect cluster order-disorder transition. The concurrence of these two transitions could imply that the structural phase transition has a close relationship with the defect order-disorder transition. Therefore, the driving force for the phase transition of Fe_{1-x}O from cubic to rhombohedral probably results from the magnetic and elastic energy interactions of FeO matrix and the larger disordered defect clusters (after the order-disorder defect cluster transition). However, the solidification of the medium after ~ 12 GPa may also induce the stress in the cell to cause peaks broadening around 14.0 GPa, an experiment with a better medium like He are desired to confirm the conjecture.

The twinning interfaces are likely to develop from the atomic planes that have large defect cluster aggregation, but the detailed structure and magnetism of the defect cluster is subject to further investigation. Since it is observed that the pressure for 111 peak broadening is sensitive to hydrostaticity,^{20,23} it is believed that the order-disorder transition pressure may also vary with pressure media.

ACKNOWLEDGMENTS

We are grateful to O. Degtyareva for help with the data analysis, and T. R. Welberry, W. Schweika, and P. Chow for valuable discussions. We also thank M. Phillips for help with the manuscript and S. Jacobsen for kindly providing the samples. This work was supported by NSF and DOE grants. HPCAT is a collaboration among the Carnegie Institution, Lawrence Livermore National Laboratory, the University of Hawaii, the University of Nevada Las Vegas, and the Carnegie/DOE Alliance Center (CDAC). The Advanced Photon Source is supported by the U. S. Department of Energy, Office of Science, Office of Basic Energy Sciences, under Contract No. W-31-109-Eng-38.

*Corresponding author. Email address: yding@hpcat.aps.anl.gov

¹F. Koch and J. B. Cohen, *Acta Crystallogr., Sect. B: Struct. Crystallogr. Cryst. Chem.* **B25**, 275 (1969).

²T. R. Welberry and A. G. Christy, *Phys. Chem. Miner.* **24**, 24 (1997).

³R. E. Cohen, I. I. Mazin, and D. G. Issak, *Science* **275**, 654 (1997).

⁴C. G. Shull, W. A. Strauser, and E. O. Wollan, *Phys. Rev.* **83**, 333 (1951).

⁵H. K. Mao, J. Shu, Y. Fei, J. Hu, and R. J. Hemley, *Phys. Earth Planet. Inter.* **96**, 135 (1996).

⁶T. Yagi, T. Suzuki, and S.-i. Alkimoto, *J. Geophys. Res.* **90**, 8784 (1985).

⁷J. Shu, H. K. Mao, J. Hu, Y. Fei, and R. J. Hemley, *Neues Jahrb. Mineral., Abh.* **172**, 309 (1998).

⁸Y. Fei and H. K. Mao, *Science* **266**, 1678 (1994).

⁹A. K. Cheetham, B. E. F. Fender, and R. I. Taylor, *J. Phys. C* **4**, 2160 (1971); C. R. A. Catlow and B. E. F. Fender, *ibid.* **8**, 3267 (1975); B. Anderson and J. O. Sletnes, *Acta Crystallogr., Sect. A: Cryst. Phys., Diffr., Theor. Gen. Crystallogr.* **33**, 268 (1977); J. R. Gavarrri, C. Carel, and D. Weigel, *J. Solid State Chem.* **29**, 81 (1979).

¹⁰P. Buseck, J. M. Cowley, and L. Eyring, *High-Resolution Transmission Electron Microscopy and Associated Techniques* (Oxford University Press, New York, 1988).

¹¹H. Tajiri, O. Skata, and T. Takahashi, *Appl. Surf. Sci.* **234**, 403 (2004).

¹²M. Holt, Z. Wu, Hawoong Hong, P. Zschack, P. Jemian, J. Tischler, Haydn Chen, and T.-C. Chiang, *Phys. Rev. Lett.* **87**, 255501 (2001).

¹³D. B. Williams and C. B. Carter, *Transmission Electron Microscopy: A Textbook For Materials Science* (Plenum Press, New

- York, 1996).
- ¹⁴B. Simons, Year Book - Carnegie Inst. Washington **79**, 376 (1980).
- ¹⁵A. P. Hammersley, S. O. Svensson, M. Hanfland, A. N. Fitch, and D. Häusermann, High Press. Res. **14**, 235–248 (1996).
- ¹⁶A. Yamamoto, Acta Crystallogr., Sect. B: Struct. Crystallogr. Cryst. Chem. **B38**, 1451–1456 (1982).
- ¹⁷A. K. Singh, J. Appl. Phys. **73**, 4278–4286 (1993).
- ¹⁸A. K. Singh and C. Balasingh, J. Appl. Phys. **75**, 4956 (1994).
- ¹⁹C. R. A. Catlow and B. E. F. Fender, J. Phys. C **8**, 3267 (1975).
- ²⁰H. Camilla, S. Stølen, M. Hanfland, and R. A. Catlow, Phys. Chem. Chem. Phys. **2**, 5333–5340 (2000).
- ²¹W. Schweika, A. Hoser, M. Martin, A. E. Carlsson, Physica B **213**, 570–572 (1995).
- ²²J. Zhang, Phys. Rev. Lett. **84**, 507 (2000).
- ²³Y. Fei, *A Tribute to Roger G. Burns*, edited by M. D. Dyar, C. MaCammon, and M. W. Schaefer, The Geochemical Society (St. Louis, 1996), pp. 243–254.
- ²⁴Y. Ding, J. Xu, C. T. Prewitt, R. J. Hemley, H. K. Mao, J. A. Cowan, J. Zhang, J. Qian, S. C. Vogel, and Y. Zhao, Appl. Phys. Lett. **86**, 052505 (2005).
- ²⁵V. V. Struzhkin, H. K. Mao, J. Hu, M. Schwoerer-Böhning, J. Shu, R. J. Hemley, W. Strurhahn, M. Y. Hu, E. E. Alp, P. Eng, and G. Shen, Phys. Rev. Lett. **87**, 055501 (2001).
- ²⁶A. P. Kantor, S. D. Jacobsen, I. Y. Kantor, L. S. Dubrovinsky, C. A. McCammon, H. J. Reichmann, and I. Goncharenko, Phys. Rev. Lett. **93**, 215502 (2004).
- ²⁷D. V. Dimitrov, K. Unruh, and G. C. Hadjipanayis, Phys. Rev. B **59**, 14499 (1999).